Eur. Phys. J. A **10**, 373–379 (2001)

THE EUROPEAN PHYSICAL JOURNAL A

Measurement of fusion excitation functions of ^{27,29,31}Al + ^{197}Au

Y.X. Watanabe[1,a,b], A. Yoshida[2], T. Fukuda[3,c], T. Sekine[4,d], Y. Watanabe[2], H. Ikezoe[5], Y. Nagame[5], T. Ikuta[5], I. Nishinaka[5], Y. Mizoi[3,e], J. Nakano[3,f], M. Hirai[1,g], H. Sakurai[1], H. Kobinata[1,h], Y. Pu[2,i], K. Kimura[6], and M. Ishihara[1,2]

[1] Department of Physics, Faculty of Science, University of Tokyo, 7-3-1 Hongo, Bunkyo, Tokyo 113-8654, Japan
[2] RIKEN (The Institute of Physical and Chemical Research), 2-1 Hirosawa, Wako, Saitama 351-0198, Japan
[3] Institute for Nuclear Study, University of Tokyo (INS), 3-2-1 Midori-cho, Tanashi, Tokyo 188-0002, Japan
[4] Faculty of Science, Tokyo Institute of Technology, 2-12-1 Ookayama, Meguro, Tokyo 152-8551, Japan
[5] Japan Atomic Energy Research Institute, 2-4 Shirane, Tokai-mura, Naka-gun, Ibaraki 319-1195, Japan
[6] Faculty of Engineering, Nagasaki Institute of Applied Science, 536 Aba-machi, Nagasaki, Nagasaki 851-0193, Japan

Received: 13 March 2001 / Revised version: 20 April 2001
Communicated by C. Signorini

Abstract. A systematic study of the sub-barrier fusion reactions with neutron-rich projectiles has been carried out for three isotopes ^{27,29,31}Al bombarding a ^{197}Au target. A target chamber equipped with a target stack and sets of MWPC was employed in order to enhance the efficiency of the radioactive beam experiment. Coupled-channel calculations including the quadrupole excitations do not well fit the measured fusion excitation functions, whereas flat barrier distributions to represent the coupling to the neutron transfer largely account for the observed enhancement of the sub-barrier fusion cross-sections.

PACS. 25.60.Pj Fusion reactions – 25.70.Jj Fusion and fusion-fission reactions

1 Introduction

It is known that heavy-ion fusion cross-sections are strongly enhanced in the energy region near and below the classical fusion barrier as compared to the expectation from the one-dimensional barrier penetration model [1]. Various mechanisms have been proposed to explain such enhancement of the sub-barrier fusion cross-sections: zero-point motion of collective surface vibration [2], coupling to inelastic excitation and nucleon transfer channels [3], and neck formation between the colliding nuclei [4]. These effects can also be treated in terms of distribution of fusion barriers [5,6].

The advent of radioactive beams has brought a renewed interest in the study of the sub-barrier fusion, since very neutron-rich projectiles may give rise to unique possibilities of extra enhancement. Loosely bound neutron-rich nuclei exhibit several characteristic features. Firstly, a neutron density distribution extended far beyond the range of normal nuclei is often manifested in the so-called neutron halo or skin nuclei [7]. Such an extended distribution naturally leads to a larger Coulomb barrier radius and hence to a lowered height of the fusion barrier, resulting in the enhancement of the sub-barrier as well as the above-barrier fusion cross-sections [8,9]. Besides, one may expect significant dynamical effects in the entrance channel, which can be induced through the coupling to the inelastic reaction processes. In this regard, the soft dipole excitation [8,10] and breakup reaction [11–15] would be important, since they can be favorably promoted for loosely bound neutron-rich nuclei. Finally, the coupling to neutron transfer channels would be also important for the neutron-rich nuclei, whose small neutron separation energies could help to lower the fusion barrier [16].

In the present work, a systematic study of the fusion excitation function has been performed for the three

[a] *Present address:* RIKEN
[b] e-mail: `yutaka@rarfaxp.riken.go.jp`
[c] *Present address:* High Energy Accelerator Research Organization (KEK), 1-1 Oho, Tsukuba, Ibaraki 305-0801, Japan
[d] *Present address:* Tokai Works, Japan Nuclear Cycle Development Institute, 4-33 Muramatsu, Tokai-mura, Naka-gun, Ibaraki, 311-1194 Japan
[e] *Present address:* RIKEN
[f] *Present address:* KEK
[g] *Present address:* National Institute of Radiological Sciences, 4-9-1 Anagawa, Inage, Chiba, 263-8555, Japan
[h] *Present address:* Micro-Fabrication Process Develop. Lab., ULSI Device Development Laboratories, NEC Corporation, 1120 Shimokuzawa, Sagamihara, Kanagawa 229-1134, Japan
[i] *Present address:* Quantum Instruments and Technology Group, Electromechanical System Dept., Advanced Technology R&D Center, Mitsubishi Electric Corporation, 8-1-1 Tsukaguchi-Honmachi, Amagasaki, Hyogo 661-8661, Japan

isotopes ^{27,29,31}Al with a common target nucleus of ^{197}Au. This combination of projectiles was chosen because the two-neutron separation energy S_{2n} varies widely among these isotopes; the values of S_{2n} are 24.4, 17.2 and 12.9 MeV for ^{27,29,31}Al, respectively. For the isotopes studied, the effects of the extended neutron distribution and of the breakup process may be weak since their binding is not extremely loose. On the other hand, the influence of the neutron transfer process may be depicted through the wide variation of the separation energy among the three isotopes.

Recently, fusion excitation functions were studied at MSU for the stable ^{32}S and unstable ^{38}S projectiles with the ^{181}Ta target nucleus [17]. The data were fitted to coupled-channel calculations including the deformation of the target nucleus, the excitation of the first quadrupole and octupole states of the projectile nuclei, and the excitation of the low-lying states of the ground state rotational band of the target nucleus. The data were reproduced fairly well by significantly changing the depth of the nuclear potential between the two systems studied. On the other hand, the low-energy data only reached the region of the classical barrier, corresponding to cross-sections not lower than ∼100 mb. In order to investigate the effect of neutron transfer, the data well below the barrier are most sensitive. Thus, we have extended the present measurement to the region of ∼10 mb.

The experiment was performed by using radioactive beams of ^{29,31}Al. To enhance the experimental efficiency, a package of many target foils was employed. The data were first compared with the result of a standard theoretical analysis using the coupled-channel code CCDEF [18], where the effects of inelastic channels were quantitatively treated. The significant discrepancies arising from the comparison were then discussed in relation to possible effects of neutron transfer [5].

2 Experimental procedure

The experiments with unstable nuclei ^{29,31}Al were performed using the projectile fragment separator RIPS [19] at RIKEN. Beams of ^{29}Al and ^{31}Al were produced in the fragmentation of a primary beam of 90 MeV/A ^{40}Ar, which impinged on a production target consisting of a Be plate with 2.5 mm thickness. The radioactive residual fragments were separated through two dipole magnets with an achromatic degrader placed in between. The beams were transmitted to the target area through the two focal points, F2 and F3 separated by 5.78 m along the beam line. Figure 1 schematically shows the experimental setup used to measure the fusion cross-sections. An Al plate with 0.98 mm (0.85 mm) thickness for the ^{29}Al (^{31}Al) beam was installed near F2 to bring down the beam energy to the appropriate region for the fusion reaction. The energy of the beam particle was determined event by event, measuring the time of flight (TOF) between F2 and F3. For this purpose a thin plastic scintillator with 0.5 mm thickness and a microchannel plate detector (MCP) with a Formvar film coated with ∼200 μg/cm^2 Au were placed at F2 and

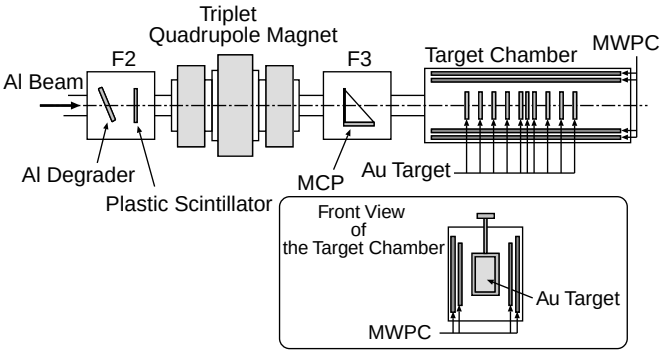

Fig. 1. Schematic drawing of the experimental setup. Lower panel shows a front view of the target chamber.

F3, respectively. After passing through the degrader and the TOF detectors as well as the production target and the achromatic degrader, the beam of ^{29}Al (^{31}Al) had a typical intensity of 1×10^5 cps (3×10^4 cps) and a wide energy spread ranging from 161 MeV (119 MeV) to 216 MeV (200 MeV) at the half maximum intensity. Pile-up events were rejected by a logic circuit with 300 ns rejection capability, which ensured one-to-one correspondence between an injected particle and its reaction event. Impurity nuclei in the ^{29,31}Al beam were eliminated using information of two TOFs: one between F2 and F3, the other between the Be production target and F2.

The target chamber was placed downstream F3. It accommodated both a multi-fold target and two pairs of MWPC, and was filled with a gas mixture of helium (40 mbar) and isobutane (10 mbar) for the wire detectors. The multi-fold target was employed to increase the event rate considerably. It consisted of a stack of 10 foils of Mylar-backed Au, which were separated from their adjacent neighbors by 6 cm (in part 3 cm) along the beam direction. These foils were obtained by evaporation onto Mylar films and had an area of 64(H)×38(W) mm^2. The areal density of Au ranged from 270 μg/cm^2 to 460 μg/cm^2, while the Mylar had a thickness of 1 μm.

As the beam went through the target chamber, it was further decelerated by the target foils and detector gas. Separate runs were carried out to observe the shift of the beam energy through the chamber by placing a silicon solid state detector at the back of each target foil. The energies at different target foil positions were then determined as functions of TOF for the incoming particle. The accuracy of the beam energy thus determined was ±0.9 MeV at the first target position and ±1.5 MeV at the last target position. The broad distribution of the beam energy over the target foils was useful to obtain the fusion excitation function at a time.

Compound nuclei produced by the fusion reactions resulted in fission with emission of two fragments. These fragments were detected with pairs of MWPCs placed on both sides of the target stack. Each pair comprised inner and outer MWPCs, which, respectively, had six and twelve resistive anode wires stretched along the beam direction. The wires were separated at intervals of 12 mm to

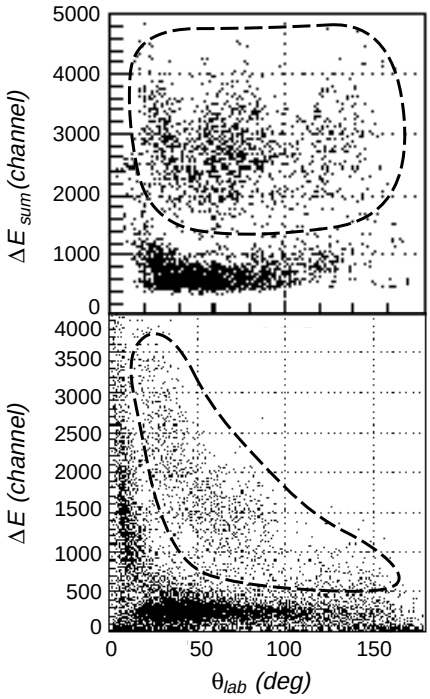

Fig. 2. Two-dimensional plots of $\theta_{\rm lab}$-ΔE for the ^{29}Al + ^{197} Au reaction, where $\theta_{\rm lab}$ and ΔE show the zenithal angle in the laboratory system, and the energy loss through an MWPC for the ejected particles, respectively. The lower panel shows the energy loss of the single particle, whereas the upper panel shows the summation of the energy loss of the two particles detected in coincidence by the MWPCs on both sides. The dashed curves indicate the fission fragments.

determine the vertical coordinate of the impinging fragment, while the coordinate along the beam direction was determined from the charges collected at both ends of the anode wires. Fusion-fission events were separated by imposing a condition, that the two pairs of MWPCs were hit in coincidence. The target foil at which the reaction occurred was identified from the tracks of two fragments determined by the pairs of MWPCs. Figure 2 shows a typical two-dimensional plot for the ^{29}Al + ^{197} Au reaction analyzed. Background or spurious events due to elastic scattering and other reactions were easily separated by incorporating energy losses at the MWPCs, the ejection angle of each fragment, and the opening angle of the two fragments.

The fusion cross-sections were deduced by correcting for the detector acceptance, assuming a fission angular distribution of the form of $1/\sin\theta_{\rm cm}$, where $\theta_{\rm cm}$ shows zenithal angle of the fragment in the center-of-mass system. This angular distribution was verified in the range of $30^\circ \leq \theta_{\rm cm} \leq 160^\circ$ for ^{27}Al + ^{197} Au, which was measured at JAERI as described in detail below. Because PACE2 [20] simulations show that the contribution of evaporation channels is less than 0.1% in the measured energy region, the fusion-fission cross-sections are considered as the total fusion cross-sections.

The fusion reaction with the stable nucleus ^{27}Al was performed in two different ways. The first experiment was performed using a 182.3 MeV ^{27}Al beam from the RIKEN AVF cyclotron. In this case, the same setup of the target and MWPC system as used for the radioactive beams was employed. The target consisted of twenty foils of Au with areas of 28(H)×22(L) mm^2, and the areal densities ranging from 68.8 μg/cm^2 to 190.3 μg/cm^2. These foils were backed by Mylar films of 0.58 μm thickness. In contrast to the case of the radioactive beams, the incident beam was monochromatic so that the energy was fixed at each target position. On the other hand, the energy varied along the chamber as the particle lost the energy by the upstream foils and detector gas. Thus, the fusion cross-sections at twenty different energy points were measured at a time.

The second experiment was performed to provide a reference for the calibration of the MWPC detection system. It was, thus, performed with a standard method so as to obtain an absolute magnitudes of cross-sections. In this experiment, the ^{27}Al beam was provided by the 20 MV tandem accelerator of the Japan Atomic Energy Research Institute (JAERI), and a single target foil of Au with a thickness of ∼480 μg/cm^2 was irradiated. The beam energy was varied stepwise from 109.6 MeV to 137.5 MeV in the center-of-mass system. Fission fragments were detected in singles with a large ionization chamber [21], which comprised a ΔE-E telescope with seven surface barrier silicon detectors on the rear plate of the chamber. The silicon detectors were placed at every 15°, each spanning about 2.9°. The angular distribution from 22.6° to 156.8° in the laboratory system was obtained by moving the chamber. The fusion cross-sections were deduced by normalizing to the Rutherford scattering cross-sections obtained by a surface barrier silicon detector placed at 43.8° in the laboratory system, and by fitting the angular distribution to the shape of $1/\sin\theta_{\rm cm}$.

The following has been found through the two experiments on ^{27}Al. The fusion cross-sections obtained from the second experiment nicely agreed with the Bass model calculation [22] for the wide energy region well above the fusion barrier (∼117 MeV). The excitation functions of the two experiments are well scaled to each other over the entire energy range, indicating that the counting efficiency does not vary with the beam energy. On the other hand, absolute magnitudes of the cross-sections for the first experiment are smaller by about 40% when the counting efficiency of the MWPC system was assumed to be simply due to the acceptance as determined by the geometry.

3 Result and discussion

Figure 3 shows the fusion excitation functions for the three Al isotopes detected with the chamber of the multifold target and MWPC system. In order to facilitate the comparison among three isotopes, the energy $E_{\rm cm}$ in the center-of-mass system is shown in the unit of the fusion barrier $V_{\rm B}$ and the cross section σ is shown in the unit of $\pi R_{\rm B}^2$, where $R_{\rm B}$ is the barrier radius. The $V_{\rm B}$ and $R_{\rm B}$ were calculated with the Bass potential [23]; the values

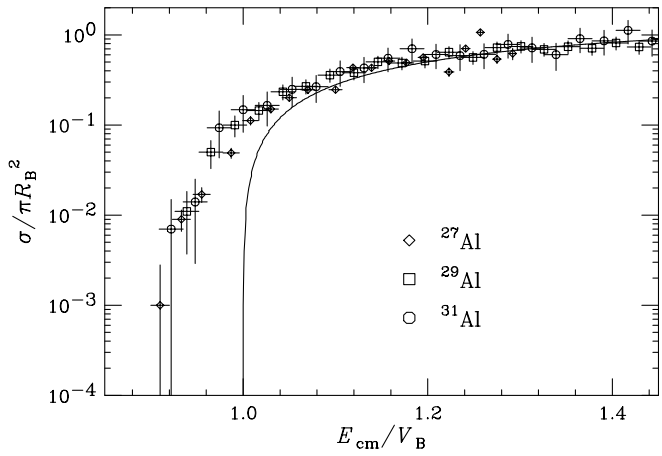

Fig. 3. Measured fusion excitation functions of ^{27,29,31}Al + ^{197}Au. The abscissa shows the energy in the center-of-mass system in the unit of the fusion barrier V_B. The ordinate shows the fusion cross-sections in the unit of πR_B^2, where R_B is the barrier radius. The V_B and R_B were calculated with the Bass potential [23]. The solid curve represents the Bass model calculation [22].

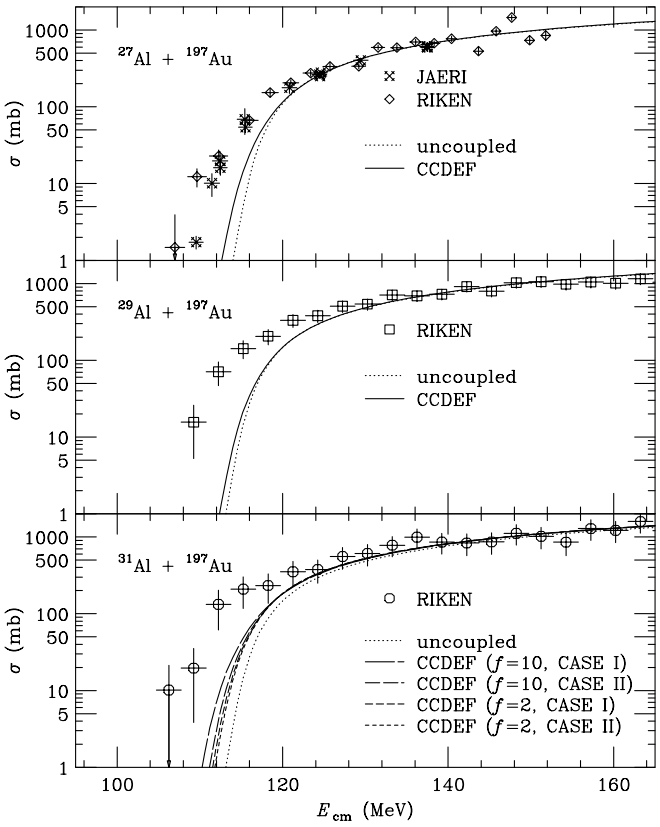

Fig. 4. Comparison of the experimental fusion excitation functions with coupled-channel calculations. The solid and dashed curves are the calculations with inelastic channels in table 1. The dotted curves indicate the uncoupled case. See text for details.

of V_B for ^{27,29,31}Al are 117.5, 116.3 and 115.2 MeV, respectively, the values of R_B for ^{27,29,31}Al are 11.7, 11.9 and 12.0 fm, respectively. For all the spectra, the normalization was made so as to reach a best fit to the results of Bass model calculations over the high-energy region. The horizontal bars across the experimental points indicate the energy bin size for the data of radioactive ^{29,31}Al, while those for ^{27}Al represent the energy accuracy in the measurement. The energy bin size was determined to be 3 MeV according to the inaccuracy of the beam energy at the last target position, where the largest uncertainty was expected. The solid curve indicates the Bass model calculation [22]. Apparently the observed cross-sections near and below the fusion barrier are significantly enhanced for all the three spectra, whereas isotopic variation could not be seen clearly.

In order to elucidate the origin of the sub-barrier enhancement, the data are first compared with the coupled-channel calculations using the CCDEF code [18], which may properly account for the effects of coupling to inelastic channels. The code involves a tunable parameter dv to adjust the depth of the nuclear potential. The value of $dv = 10$ gave a good overall fit to the data in the energy range $E_{cm} \geq 120$ MeV for all the three reaction systems. This value was, thus, employed for the further analysis. Quadrupole inelastic channels of both the projectile and target nuclei as well as the static quadrupole deformation of the target nucleus were included in the calculation. Table 1 lists the excited states and the relevant parameters involved in the calculations [24,25]. The parameters are experimentally known for ^{27}Al and ^{29}Al. On the other hand, only the energies of the excited states are known for ^{31}Al.

To make the estimation for ^{31}Al, we assumed that the three lowest excited states are coupled to the ground state by quadrupole vibrational modes. As listed in table 1, we considered two plausible combinations of spin assignments for the four levels, corresponding to the maximal and minimal contribution of the spin factor. The $B(E2)\uparrow$ strengths were also assumed and given in terms of the expression $B(E2)\uparrow = f \times \{\frac{2J_x+1}{2J_g+1} B_W(E2)\}$, where $B_W(E2)$ represents the Weisskopf unit. For comparison, the f values are 7.92 and 7.83, respectively, for the first and second levels of ^{27}Al, while they are 4.45 and 5.80 for ^{29}Al. Thus, a common f value was simply taken for the three transitions of ^{31}Al. The magnitudes were then chosen in two ways as $f = 2$ or 10, representing possible lower and upper limits.

The curves thus calculated are shown in fig. 4 with solid lines for ^{27}Al and ^{29}Al and with four different dashed lines for ^{31}Al. The theoretical curves indicate appreciable enhancement for the sub-barrier cross-sections as compared to the one-dimensional barrier penetration (dotted curve). However, the magnitude of the enhancement is by far insufficient to account for the large sub-barrier cross-sections of the experimental data. Thus, the importance of the effects other than from the inelastic channels is suggested.

A further attempt to improve the fit was performed by widely changing the dv parameter. It was found that

Table 1. Inelastic channels included in the coupled-channel calculations. E_x, J, π, $B(E2)\uparrow$ and β_2 indicate the excitation energy in keV, the spin, the parity, the reduced $E2$ transition probability divided by Weisskopf unit $B_W(E2) = 5.94 \times 10^{-6} A^{\frac{4}{3}}$ e^{2}b^2, and the static quadrupole deformation parameter, respectively. In the case of ^{31}Al, it was assumed that $B(E2)\uparrow = f \times \{\frac{2J_x+1}{2J_g+1} B_W(E2)\}$, where $f = 2$ or 10, and two cases of the spin assignment were considered. See text for details.

^{27}Al			^{29}Al			^{197}Au		
E_x (keV)	J^π	$B(E2)\uparrow$ (W.u.)	E_x (keV)	J^π	$B(E2)\uparrow$ (W.u.)	E_x (keV)	J^π	$B(E2)\uparrow$ (W.u.)
0	$\frac{5}{2}^+$		0	$\frac{5}{2}^+$		0	$\frac{3}{2}^+$	$\beta_2 = -0.11$
843.8	$\frac{1}{2}^+$	2.64	1398.0	$\frac{1}{2}^+$	1.48	77.4	$\frac{1}{2}^+$	17.5
1014.5	$\frac{3}{2}^+$	5.22	1754.2	$\frac{7}{2}^+$	7.73	268.8	$\frac{3}{2}^+$	18.1
2211.1	$\frac{7}{2}^+$	20.0	2224.0	$\frac{3}{2}^+$	1.01			
2734.9	$\frac{5}{2}^+$	0.66						

^{31}Al						
E_x (keV)	CASE I			CASE II		
	J^π	$B(E2)\uparrow$ (W.u.)		J^π	$B(E2)\uparrow$ (W.u.)	
		$f = 2$	$f = 10$		$f = 2$	$f = 10$
0	$(\frac{3}{2}^+)$			$(\frac{5}{2}^+)$		
946.9	$(\frac{7}{2}^+)$	4	20	$(\frac{1}{2}^+)$	0.66	3.3
1613.1	$(\frac{5}{2}^+)$	3	15	$(\frac{3}{2}^+)$	1.3	6.7
2090.0	$(\frac{3}{2}^+)$	2	10	$(\frac{5}{2}^+)$	2	10

fair agreement with the sub-barrier data was obtained when the value of $dv = 60$ was used for ^{29}Al. However, this value largely deviates from the recommended range of $dv = -10$ to 10, and indeed results in enormously large fusion cross-sections at higher energies corresponding to ∼10% increase of the projectile radius.

Recently, CCFULL code [26] provided more exact treatment on coupled-channel calculations for fusion reactions including higher-order coupling effects. Although such calculations would possibly improve the discrepancy, the coupling to the neutron transfer channels is a major possibility among the other plausible mechanisms for the sub-barrier enhancement. This effect can be treated by an approach proposed by Stelson [5], in which the enhancement is represented in terms of distributed fusion barriers. The distribution is assumed to be a flat function, whose boundaries are correlated with the relevant two-neutron separation energies; the lower boundary B_{lo} is given by the threshold barrier B_{th}, while the upper boundary B_{up} is symmetric of B_{lo} with respect to the ion-ion potential barrier B_m. The values of B_{th} can be calculated by assuming that the neutron transfer channel opens when the target and projectile nuclei arrive at the distance R_{th}, where the barrier across the merging Woods-Saxon potentials of the colliding nuclei becomes equal to $-S_{2n}/2-4$ MeV. The threshold barrier height B_{th} is then given as the energy of the ion-ion potential at R_{th}. The threshold barriers B_{th} are defined bi-directionally, $B_{th}^{Al\to Au}$ and $B_{th}^{Al\leftarrow Au}$, corresponding to the neutron transfer from Al to Au and from Au to Al.

The barrier distributions thus obtained were shown with dashed lines in fig. 5. In calculating the barrier distributions, Woods-Saxon parameters of $V_0 = -50$ MeV, $R_0 = 1.24A^{\frac{1}{3}}$ fm and $a = 0.68$ fm were chosen and the Bass potential [23] was employed for the ion-ion potential. The distributions have the shape of two-fold flat functions dictated by the balance between $B_{th}^{Al\to Au}$ and $B_{th}^{Al\leftarrow Au}$. The former value decreases together with S_{2n} as the Al isotope becomes richer in neutrons, while the latter changes rather little for the three reaction systems. Thus, the identity of the lowest of the two changes for the different reactions as $B_{th}^{Al\to Au} > B_{th}^{Al\leftarrow Au}$ for ^{27,29}Al, and $B_{th}^{Al\to Au} < B_{th}^{Al\leftarrow Au}$ for ^{31}Al.

The values of B_{th}, B_m and $|B_{th} - B_m|_{max}$ are summarized in table 2, where $|B_{th} - B_m|_{max}$ represents the half width of the flat distribution. For all of the three reactions studied, the $|B_{th} - B_m|_{max}$ values are as large as ∼10 MeV, which represent the largest cases among the reaction systems ever studied [16]. For comparison, the barrier distributions calculated for the couplings to the inelastic channels are shown by vertical solid lines in fig. 5. These values were extracted from the CCDEF code with small modification to the code itself. Indeed, the flat distributions for the neutron transfer are so wide that they extend far beyond the boundaries of the inelastic distributions.

Table 2. Parameters in the flat barrier distribution model calculations. S_{2n}, B_{th}, B_m and R_m are the two-neutron separation energy, the threshold barrier, the classical single barrier, and the nuclei's distance where B_m is located, respectively.

System	S_{2n} (MeV)		B_{th} (MeV)		B_m (MeV)	$\pi R_m{}^2$ (mb)	$\lvert B_{th} - B_m \rvert_{max}$ (MeV)
	Al	Au	Al→Au	Al←Au			
^{27}Al + ^{197}Au	24.4	14.7	111.1	107.2	117.5	4315	10.3
^{29}Al + ^{197}Au	17.2	14.7	107.6	106.5	116.3	4419	9.8
^{31}Al + ^{197}Au	12.9	14.7	105.0	105.8	115.2	4516	10.2

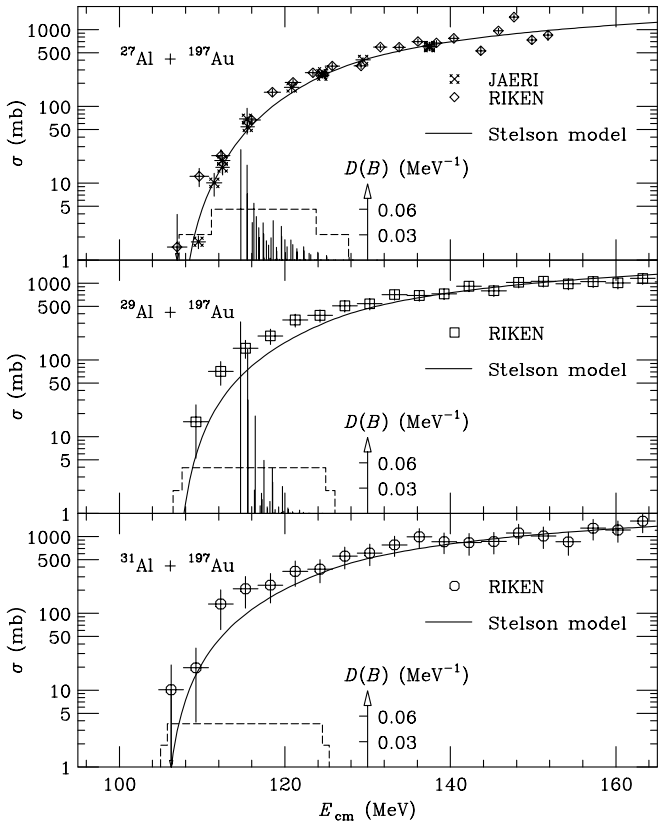

Fig. 5. Comparison of the experimental fusion excitation functions with flat barrier distribution model calculations. The solid curves are the calculations with the parameters in table 2. The dashed lines show the barrier distributions $D(B)$. The vertical solid lines show the barrier distributions calculated in CCDEF. See text for details.

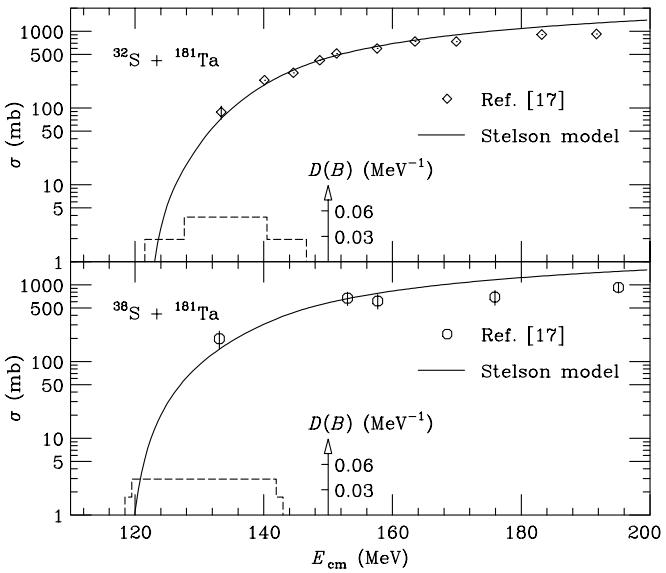

Fig. 6. Comparison of the experimental fusion excitation functions for ^{32,38}S+^{181}Ta [17] with flat barrier distribution model calculations. The solid curves are the calculations. The dashed lines show the barrier distributions $D(B)$.

The excitation functions calculated using these flat distributions are compared in fig. 5 with the experimental results. The theoretical curves exhibit sizable enhancement of sub-barrier cross-sections which greatly improves the agreement with the observed cross-sections. Because the three isotopes show the almost same barrier width $|B_{th} - B_m|_{max}$ owing to the neutron separation of the target nucleus, not so strong isotopic variation was seen in agreement with the tendency of fig. 3. By further adding the effects of inelastic channels, the remaining deficiency might be remedied.

In an attempt to examine the validity of the Stelson model, we extended the analysis to the reaction systems ^{32,38}S +^{181} Ta [17], whose $|B_{th} - B_m|_{max}$ values are as large as those of the Al reactions. Figure 6 shows a comparison of the data extracted from ref. [17] with the calculations. The excitation functions calculated with the relevant flat distributions reproduced the experimental data fairly well.

4 Summary

In summary, a systematic study of the fusion excitation function extending to the sub-barrier region has been performed for the systems of ^{27,29,31}Al +^{197} Au. The comparison of the experimental data with the coupled-channel calculation and that of the neutron transfer model of ref. [5] suggests that the neutron transfer significantly contributes to the enhancement of sub-barrier fusion cross-sections.

The effect of neutron transfer on the enhancement of the sub-barrier fusion cross-sections has been considered in early papers [5,27,16], where the treatment using the

model of Stelson yielded fairly good global agreement with a large number of reaction systems. On the other hand, some of these data as well as others were well accounted for in detail when the couplings with inelastic channels were carefully treated. Thus, the current situation has been somewhat confusing as to whether the effect of the neutron transfer is indeed important. In a recent work [28] on ^{40}Ca + ^{90,96}Zr fusion reactions, significance of multi-nucleon transfer was suggested. The present result may offer another new evidence which calls for the importance of neutron transfers.

We would like to thank the staff of RIKEN Ring Cyclotron for their operation of the accelerator. We acknowledge Dr. I. Sugai for preparing the target foils of Au filmed with Mylar.

References

1. M. Beckerman, Phys. Rep. **129**, 145 (1985).
2. H. Esbensen, Nucl. Phys. A **352**, 147 (1981).
3. C.H. Dasso, S. Landowne, A. Winther, Nucl. Phys. A **405**, 381 (1983).
4. C.E. Aguiar, V.C. Barbosa, L.F. Canto, R. Donangelo, Nucl. Phys. A **472**, 571 (1987).
5. P.H. Stelson, Phys. Lett. B **205**, 190 (1988).
6. M. Dasgupta, D. J. Hinde, N. Rowley, A.M. Stefanini, Ann. Rev. Nucl. Particle Sci. **48**, 401 (1998).
7. I. Tanihata, T. Kobayashi, O. Yamakawa, S. Shimoura, K. Ekuni, K. Sugimoto, N. Takahashi, T. Shimoda, H. Sato, Phys. Lett. B **206**, 592 (1988).
8. N. Takigawa, H. Sagawa, Phys. Lett. B **265**, 23 (1991).
9. J.A. Christley, C.H. Dasso, S.M. Lenzi, M.A. Nagarajan, A. Vitturi, Nucl. Phys. A **587**, 390 (1995).
10. C.H. Dasso, R. Donangelo, Phys. Lett. B **276**, 1 (1992).
11. M.S. Hussein, M.P. Plato, L.F. Canto, R. Donangelo, Phys. Rev. C **46**, 377 (1992).
12. N. Takigawa, M. Kuratani, H. Sagawa, Phys. Rev. C **47**, R2470 (1993).
13. C.H. Dasso, J.L. Guisado, S.M. Lenzi, A. Vitturi, Nucl. Phys. A **597**, 473 (1996).
14. K. Hagino, A. Vitturi, C.H. Dasso, S.M. Lenzi, Phys. Rev. C **61**, 037602 (2000).
15. A. Yoshida, C. Signorini, T. Fukuda, Y. Watanabe, N. Aoi, M. Hirai, M. Ishihara, H. Kobinata, Y. Mizoi, L. Mueller, Y. Nagashima, J. Nakano, T. Nomura, Y.H. Pu, F. Scarlassara, Phys. Lett. B **389**, 457 (1996).
16. D. Shapira, P. H. Stelson, Phys. Rev. C **47**, 1666 (1993).
17. K.E. Zyromski, W. Loveland, G.A. Souliotis, D.J. Morrissey, C.F. Powell, O. Batenkov, K. Aleklett, R. Yanez, I. Forsberg, M. Sanchez-Vega, J.R. Dunn, B.G. Glagola Phys. Rev. C **55**, R562 (1997).
18. J. Fernández-Niello, C. H. Dasso, S. Landowne, Computer Phys. Commun. **54**, 409 (1989).
19. T. Kubo, M. Ishihara, N. Inabe, H. Kumagai, I. Tanihata, K. Yoshida, T. Nakamura, H. Okuno, S. Shimoura, K. Asahi, Nucl. Instrum. Methods Phys. Res. B **70**, 309 (1992).
20. A. Gavron, *Computational Nuclear Physics*, edited by K. Langanke, J.A. Maruhn, S. E. Koonin, Vol. **2** (Springer-Verlag, New York, 1993) p. 108.
21. Y.H. Pu, S.M. Lee, S.C. Jeong, H. Fujiwara, T. Mizota, Y. Futami, T. Nakagawa, H. Ikezoe, Y. Nagame, Z. Phys. A **353**, 387 (1996).
22. R. Bass, Nucl. Phys. A **231**, 45 (1974).
23. R. Bass, Phys. Rev. Lett. **39**, 265 (1977).
24. R.M. Endt, Nucl. Phys. A **521**, 1 (1990).
25. Zhou Chunmei, Nuclear Data Sheets **62**, 433 (1991).
26. K. Hagino, N. Rowley, A.T. Kruppa, Computer Phys. Commun. **123**, 143 (1999).
27. P.H. Stelson, H.J. Kim, M. Beckerman, D. Shapira, R. L. Robinson Phys. Rev. C **41**, 1584 (1990).
28. H. Timmers, D. Ackermann, S. Beghini, L. Corradi, J.H. He, G. Montagnoli, F. Scarlassara, A.M. Stefanini, N. Rowley, Nucl. Phys. A **633**, 421 (1998).